Tracking of the Anterior Mitral Leaflet in Echocardiographic Sequences using Active Contours

Malik Saad Sultan[1,2] Nelson Martins[1,2,3] Diana Veiga[3,4] Manuel João Ferreira[3,4] Miguel Tavares Coimbra[1,2]

***Abstract*— Echocardiography assessment of cardiac valves plays a vital role in the diagnosis of rheumatic heart disease. In the vast majority of cases, the mitral valve gets affected, leading to the thickening of its leaflets that may result in the fusion of their tips. This changes the appearance and reduces the mobility of the leaflets, which also reduce the heart efficiency. Quantifying such parameters provides diagnostic insight. To achieve that, the first step is to identify and then track fast moving leaflets. This work is focused on Anterior Mitral Leaflet (AML) tracking. Open ended active contours are employed in this work by removing its boundary conditions. The external and internal energy of the contour is modified that extend the capture range, improve snake energy and encourages the leftmost end point of the contour to converge on the moving tip of the AML. Results show that contour points are tracked accurately with an average error of 4.9 pixels and a standard deviation of 2.1 pixels in 9 fully annotated normal sequences of real children clinical assessments.**

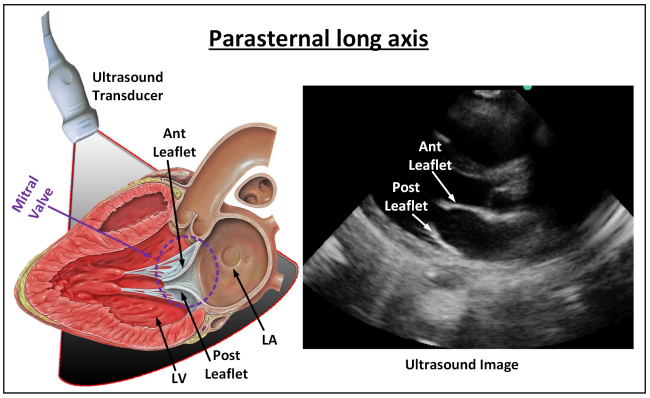

Fig. 1. Parasternal long axis view of a normal mitral valve in diastole.

I. Introduction

Rheumatic Heart Disease is one of the serious consequences of Acute Rheumatic Fever. Acute Rheumatic Fever is the inflammatory disease that usually begins in childhood, and whose repeated episodes slowly damage the valves of the heart. Since Rheumatic Heart Disease doesnt occur after the very first attack, the early detection is considered vital to define the disease burden and to control disease progression [1, 2]. Echocardiography can play a key role by providing early evidence, since one can confirm the suspected cases (valve involvement), which can be treated accordingly [3, 4].

Remnyi et al. [4] found that the mitral valve damage was dominant with or without the involvement of other valves (aortic valve, pulmonic valve and tricuspid valve). The morphological features such as thickened leaflet, fused leaflet tips, excessive leaflet tip motion and restricted leaflet motion (hockey stick like appearance) can be evaluated using echocardiography [5].

The Paresternal Long Axis (PLA) view is the most suitable view that allows us to access the mitral valve [6] (Fig. 1). The thickness, appearance, fused tips and motion of the anterior leaflet can be analysed in this view. To measure such feature, first we need to segment and then track the AML during the whole cardiac cycle.

Kass et al. [7] introduced an iterative energy minimizing process in which parametric contours evolve under the influence of image forces and the shape is controlled by an internal constraint. This contours model is known as snakes, which provide a framework that offers automatic/semi-automatic image segmentation and motion tracking.

Later on, several shortcomings of the algorithm were found such as, initialization, convergence, etc., which motivates the researchers to propose various algorithms to improve the classical snake. Cohen et al. [8] introduce a constant force term (balloon force) in the model that drives the snake points inward/outward. The advantage of the new model is to decrease the dependence of the snake on the initialization. Williams and Shah [9] proposed a greedy snake algorithm that computes the movement of individual snake points on the image plane in a discrete way instead of computing the whole snake at once. Xu and Prince [10] proposed the use of Gradient Vector Flow energy instead of classical edge energy. Proposed energy has improved the attraction range of the classical snake and thus minimizes the dependence on initialization.

Closed contours were widely used in segmentation applications, though open ended contours were occasionally employed for linear features such as road extraction, detecting coastline and their changes from satellite images, and to detect linear features from medical images [11, 12]. Depending on the nature of the application, fixed boundary condition and/or no boundary conditions were employed.

In this work, the classical snake model is modified to track thin and elongated anterior mitral leaflets in the paresternal long axis view of ultrasound images. Open ended contours were used and external energy of the model is adapted in a way that increases the range of snake and encourages the end point of the snake to stay on the tip of the anterior mitral

[1]Faculdade de Ciências, Departamento de Ciência de Computadores, Universidade do Porto, Portugal
[2]Instituto de Telecomunicações, Porto, Portugal
[3]Enermeter, Sistemas de Medição, Lda, Braga, Portugal
[4]Centro Algoritmi, University of Minho, Guimarães, Portugal

978-1-4577-0220-4/16/$31.00 ©2016 IEEE

leaflet.

This paper is organized as follows. Section 2 provides the overview of the classical snake model. Section 3 presents details of improved snake model. Section 4 reports the tracking results, and finally Section 5 concludes the paper with a discussion and future work.

II. Classical Snake

The classical snake model considers a parameterized curve $V(S) = (x(S), y(S))^T \; S \in [0,1]$ that evolves in the spatial domain. Since the proposed work deal with images, the parameterized curve has been discretized as N sample/control points. The total energy of the classical snake consists of external and internal energy (1).

$$\int_0^1 \left(\overbrace{\frac{1}{2}\left[\underbrace{\alpha \left\| \frac{\partial V}{\partial S} \right\|^2}_{Elasticity} + \underbrace{\beta \left\| \frac{\partial^2 V}{\partial S^2} \right\|^2}_{Stiffness} \right]}^{Internal} + \overbrace{E_{ext}(V)}^{External} \right) ds \quad (1)$$

The external energy is responsible to attract contour points towards the underlying image features such as edges, lines, intensity, etc. The internal energy adds shape and smoothness constraints. Internal energy typically consists of the first derivative and second derivative. The first derivative holds the contour points together and encourages points to be equally spaced (elasticity). The second derivative controls their bending (stiffness). The weighting parameters, α and β controls the relative importance of the elasticity and stiffness, respectively.

Once the total energy is formulated, the solution is obtained with an optimization method, where the total energy must be minimized. In this paper, we use the Euler Lagrange approach for optimization (2) [13].

$$\alpha \frac{\partial^2 V}{\partial S^2} - \beta \frac{\partial^4 V}{\partial S^4} - \nabla E_{ext} = 0 \quad (2)$$

III. Improved Snake Model

The proposed method will focus on tracking alone and so it assumes perfect segmentation of the AML in the first frame. In the experiments of this paper, this will be achived by manual segmentation, in order to avoid the errors of automatic segmentation which are beyond the scope of this paper. Our modified snake model is then responsible to track these points during the whole cardiac cycle. These modifications are now explained in detail.

A. Internal energy

As previously said, the internal energy is responsible to regulate the contour by imposing the elasticity and stiffness that are the first and second derivative, respectively. The weights, α and β controls the relative influence of each term (1).

Elasticity motivates the shrinking of the contour length in each iteration and given that we are using perfect initial segmentation and that the physical length of the AML does not change in the PLA view, this measure of internal energy is not adequate for our problem. Only stiffness is used that controls the bending energy of the snake. The weight β remains constant for all the contour points. Free boundary condition is used that allows the end points of the contour to move freely on the image plane to get minimum energy, promoting line contours instead of circles. However, it is bounded to remain closer to its neighbour contour point. Above boundary condition leads to N linear equations that provide us the convenient way to write in a matrix form (3). This configuration provides the ease to solve all the points simultaneously.

$$x^{t+1} = (M + \gamma I)^{-1} x^t, y^{t+1} = (M + \gamma I)^{-1} y^t$$

$$\underbrace{\begin{bmatrix} \hat{r} & q & p & & & & \\ \hat{q} & r & q & p & & & \\ p & q & r & q & p & & \\ & \ddots & \ddots & \ddots & & & \\ & & p & q & r & q & p \\ & & & p & q & r & \hat{q} \\ & & & & p & q & \hat{r} \end{bmatrix}}_{M} \begin{cases} p = \beta \\ q = -4\beta \\ r = 6\beta \\ \hat{r} = 3\beta \\ \hat{q} = -3\beta \end{cases} \quad (3)$$

Whereas, γ control the step size and is always positive and I is an identity matrix.

B. External energy

The external energy of the classical snake model is the combination of three energy functions (4).

$$E_{ext} = w_{line} E_{line} + w_{edge} E_{edge} + w_{term} E_{term} \quad (4)$$

In the above equation, the first term is the line energy that force the snake points towards the light/dark regions, the second term is the edge energy that aligns the points at higher image gradient and finally, term energy use the curvature of level lines to find termination. Whereas, $w_{line}, w_{edge}, w_{term}$ are the respective weights assigned to each of the energy terms.

In this work external image energy of the snake is modified so that it best fits with our particular application. Instead of using a simple intensity image and the edge map, we use Difference of Gaussian (DoG), which is a simplified way to approximate the Laplacian of Gaussian. DoG was found very effective in discarding high frequency details from ultrasound images [14]. DoG is divided into two main parts: pixels with positive values were characterized as high-intensity region and negative valued pixels characterized as edges (5) (Fig. 2). Obtained edges are wider which increases the capture range and intensity regions are enhanced and well localized that encourage contour points to be aligned exactly in the middle of the AML.

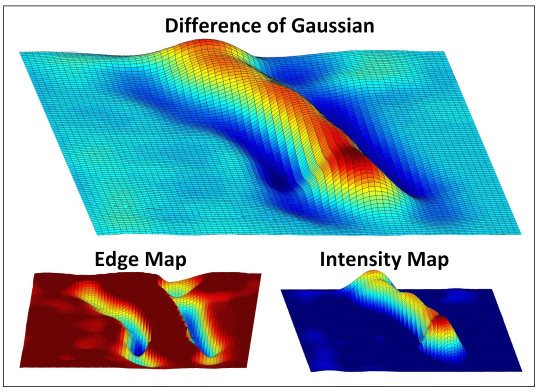

Fig. 2. Surf plots: DoG of AML region of grayscale image. Positive valued pixels (intensity map), negative valued pixels (edge map).

$$\begin{aligned} E_{DoG\_line} &= I \times (G_{\sigma_1} - G_{\sigma_2}) \quad DoG \geq 0 \\ E_{DoG\_edge} &= I \times (G_{\sigma_1} - G_{\sigma_2}) \quad DoG < 0 \end{aligned} \tag{5}$$

In the above equation, the image is convolved with the difference of Gaussian kernels of width σ_1 and σ_2 whereas, $\sigma_2 > \sigma_1$. In this work, we used the Gaussian filter of size 20 with sigma 8 and 10, obtained empirically in pilot tests.

To obtain better tracking performance, end points of the contour are encouraged to continuously follow the tip of the AML. To achieve this, cornerness energy is used, instead of line or edge energy, that encourages end points to stay on the AML tip. Several key methods such as edge-related corner, topology corner and auto-correlation were tested for our specific images. Kitchen et al. [15] Proposed edge-related cornerness measure that defines the change in gradient direction and magnitude along the edge map. The algorithm is very sensitive to noise, unstable and not well localized at blurred edges. Deriche et al [16] proposed a topology related scale-space cornerness measure. His method intelligently merges the useful property of the Laplacian (zero at the corners) and Beaudets measure (positive maximum at corner) [17]. The method was found very unstable in noisy images and extremely slow.

The methods based on auto-correlation were found quite satisfactory, thus used in this work. Moravec [18] had explored that the maximum intensity variation in various directions within the local window represents a corner. However, he was looking for a distinct region not specifically the corners. Later on, Harris et al. [19] has improved his approach by proposing analytic expansion of the shift (6).

$$S = \sum_x \sum_y \underbrace{w(x,y)}_{window} \left(\underbrace{I(x+u, y+v)}_{shifted\_intensity} - \underbrace{I(x,y)}_{intensity} \right)^2 \tag{6}$$

Window function can be a Gaussian or rectangle at position x, y. (u, v) shows a small displacement in all directions that somehow estimate the intensity difference. After applying Taylor series expansion and arithmetic operations, we get the covariance matrix A (7).

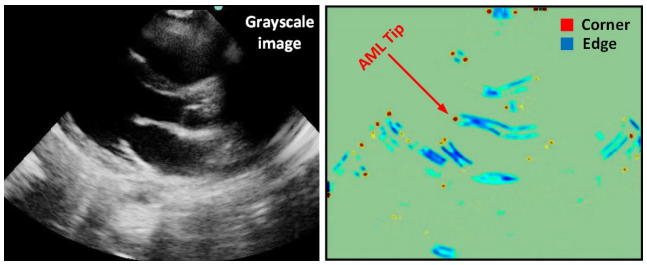

Fig. 3. Harris Cornerness measure (E_{Harris}), shows corners in Red and edges in Blue

$$A = \sum_x \sum_y w(x,y) \begin{bmatrix} I_x^2 & I_x I_y \\ I_x I_y & I_y^2 \end{bmatrix} \tag{7}$$

In this work, E_{DoG_line} image is convolved with filter $[-8\ 0\ 8]$ to get the derivatives. The derivatives are then smoothed with a Gaussian filter of size 10 and sigma 3. Finally, the cornerness measure is evaluated using (8) (Fig. 3)

$$E_{Harris} = det(A) - k(trace(A))^2 \tag{8}$$

The modified external energy of the snake is (9)

$$\begin{aligned} E_{ext} = w_{harris} E_{harris} - w_{DoG\_line} E_{DoG\_line} \\ + w_{DoG\_edge} E_{DoG\_edge} \end{aligned} \tag{9}$$

This external energy affect the snake points in a very particular way. The modified edge and intensity snake energy provide an attraction force that attracts all the points except the ones close to the AML tip (10).

$$\begin{aligned} x_S^{t+1} &= \gamma x_S^t + \left((f_x)_{DoG\_line} + (f_x)_{DoG\_edge} \right) \\ y_S^{t+1} &= \gamma y_S^t + \left((f_y)_{DoG\_line} + (f_y)_{DoG\_edge} \right) \end{aligned} \tag{10}$$

Whereas, γ is the step size, f_x and f_y are the derivatives with respect to x and y. First two points of the contour are forced to move towards the tip of AML (11).

$$\begin{aligned} x_U^{t+1} &= \gamma x_U^t + (f_x)_{Harris} \\ y_U^{t+1} &= \gamma y_U^t + (f_y)_{Harris} \end{aligned} \tag{11}$$

IV. Results

A. Materials

In one of the activities of Real Hospital Português, in Recife, Brazil, a dataset of ultrasound mitral valve videos has been collected for the purposes of screening acute rheumatic fever in children. The data was collected using a M-Turbo model by SonoSite ultrasound system, with C11x transducer (5-8 MHz). Nine of these exams were fully annotated (manual segmentation of all frames) using support software and were used to test the novel algorithm proposed in this work. These nine videos include a total of 1137 frames with dimensions of $[351 \times 441]$.

B. Tracking results

The proposed algorithm used the manual annotation as its contour initialization for the first frame of every video sequence. The algorithm manages to handle small to medium frame to frame displacement. However, the algorithm fails to track if the displacement is very high (about 33 pixel). The Hausdorff distance error between the set of manually annotated points (GS) and snake control points (SEG) is calculated (12).

$$\begin{cases} d_{GS\to SEG} = min\{GS, SEG\} \\ d_{SEG\to GS} = min\{SEG, GS\} \\ A = avg\{d_{GS\to SEG}\} \\ B = avg\{d_{SEG\to GS}\} \end{cases} \tag{12}$$

$$Error = max(A, B)$$

The algorithm is also compared with the classical snake approach exhibiting superior performance (table. 1).

TABLE I
TRACKING ERROR (PIXEL)

Video No.	***No. Of Frames***	Our Approach	Kass Approach
		Avg / STD *Error (PX)*	***Avg / STD*** *Error (PX)*
1	131	5.32 / 1.89	6.08 / 3.26
2	360	4.6 / 1.8	5.7 / 1.85
3	66	5.22 / 2.4	7.84 / 2.47
4	131	4.33 / 1.81	6.7 / 1.67
5	66	5.6 / 4.06	7.66 / 3.95
6	66	5.74 / 1.56	5.15 / 2.19
7	120	4.95 / 1.96	5.61 / 1.66
8	66	4.97 / 2.27	6.1 / 1.94
9	131	3.67 / 1.72	5.56 / 2.45
Total	**1137**	**4.93 / 2.16**	**6.26 / 2.38**

Although the used dataset is limited to nine videos, all results showed that snake points converged and were tracked accurately, with very small differences to the manual annotation.

V. DISCUSSION AND FUTURE WORK

The classical snake model was successfully modified for better performance in the specific scenario of mitral valve tracking in ultrasound images. Exploiting specific characteristics of the scenario led to a reformulation of both the internal (open contours, removal of elasticity) and external energy (DoG energy, cornerness energy for the tip of the valve) of classical snakes seems like a promising avenue to address the problem of automatic mitral valve tracking, hopefully paving the way for computer assisted decision systems that can be deployed in the field.

This promising avenue will be addressed in future work, namely the addition of a contour stretching penalty given that the valves length does not change significantly duing the video, as well as the better exploration of the visual characteristics near other sections of the valve such as the bright line nature of the central section, and the cardiac wall junction of the rightmost valve end.

ACKNOWLEDGEMENT

This article is a result of the project (NORTE-01-0247-FEDER-003507 - RHDecho), supported by Norte Portugal Regional Operational Programme (NORTE 2020), under the PORTUGAL 2020 Partnership Agreement, through the European Regional Development Fund (ERDF). This work is also funded by the Fundação para a Ciência e Tecnologia (FCT) grant no: PD/BD/105761/2014 and has contributions from the project NanoSTIMA , NORTE-01-0145-FEDER-000016, supported by Norte Portugal Regional Operational Programme (NORTE 2020), through Portugal 2020 and the European Regional Development Fund (ERDF).

REFERENCES

[1] A. Bisno, E. G. Butchart and et al. Rheumatic fever and rheumatic heart disease, Who Tech. Rep. Ser., pp. 9231122, Nov. 2001.

[2] J. R. Carapetis The stark reality of rheumatic heart disease, European Heart Journal, vol. 36, no. 18, pp. 10701073, May 2015

[3] E. Marijon, D.S. Celermajer and et al. Rheumatic heart disease screening by echocardiography: the inadequacy of World Health Organization criteria for optimizing the diagnosis of subclinical disease, Circulation, vol. 120, no. 8, pp. 663668, Aug 2009

[4] B. Remenyi, N. Wilson and et al. World heart federation criteria for echocardiographic diagnosis of rheumatic heart disease an evidence-based guideline, Nat. Rev. Cardiol., vol. 9, no. 5, pp. 297309, Feb. 2012

[5] Asberaud, Mitral stenosis assessment, Stanford university, July 2009

[6] A.S. Omran, A.A. Arifi, A.A. Mohamed, Echocardiography of the mitral valve, Journal of the Saudi Heart Association, vol. 22, no. 3, pp. 165170, Feb. 2010

[7] M. Kass, A. Witkin, D. Terzopoulouse, Snakes : active contour model, Intl journal of Computer Vision, vol. 1, no. 4, pp. 321331, Jan. 1988

[8] L. D. Cohen, On active contour models and balloons, CVGIP: Image Understanding, vol. 53, no. 2, pp. 211218, 1991

[9] D. J. Williams, M. Shah, A Fast Algorithm for Active Contours and Curvature Estimation, CVGIP: Imag. Under., Vol. 55, No. 1, pp. 14-26, 1992.

[10] C. Xu, J. Prince, Snakes, shapes, and gradient vector flow. IEEE Trans. of Image Processing, Vol. 7, No. 3, pp. 359-369, March 1998.

[11] M. Shemesh, O. Ben-Shahar, Free Boundary Conditions Active Contours with Applications for Vision, Intl Conf. on Advances in visual computing, pp. 180-191, 2011

[12] W. M. Neuenschwander, et al., Ziplock snakes, Intl Journal of Computer Vision, Vol. 25, No. 3, pp. 191-201, 1997.

[13] J. Ivins, John Porrill, Everything you Always Wanted to Know About Snakes (but were afraid to ask) , Artificial Intelligence Vision Research Unit, University Of Sheffield, March 2000

[14] M. W. Davidson, M. Abramowitz "Molecular Expressions Microscopy Primer: Digital Image Processing Difference of Gaussians Edge Enhancement Algorithm, Olympus America Inc., and Florida State University

[15] L. Kitchen, A. Rosenfeld, Gray-level corner detection, Pattern Recognition Letters 1, pp. 95-102, 1982

[16] R. Deriche, G. Giraudon, A computational approach for corner and vertex detection, Intl Journal of Computer Vision, Vol. 10, No. 2, pp. 101-124, 1993

[17] P.R. Beaudet, Rational invariant image operators, 4th Intl Conf. on Pattern Recognition, pp. 579-583, 1978

[18] H.P. Moravec, Towards automatic visual obstacle avoidance, 5th Intl Joint Conf. On Artifcial Intelligent, pp. 584, 1977

[19] C. Harris, M. Stephens, A combined corner and edge detector, Alvey vision Conf., 1988